Linear collisionless dynamics of the GAM with kinetic electrons: comparison simulations/theory

V. Grandgirard, X. Garbet, Ch. Ehrlacher, Y. Asahi, E. Cashera, Guilhem Dif-Pradalier, P. Peter Donnel, Ph. Ghendrih, G. Latu, Ch. Passeron, et al.

▶ **To cite this version:**

V. Grandgirard, X. Garbet, Ch. Ehrlacher, Y. Asahi, E. Cashera, et al.. Linear collisionless dynamics of the GAM with kinetic electrons: comparison simulations/theory. 2018. cea-01913153

HAL Id: cea-01913153
https://cea.hal.science/cea-01913153

Preprint submitted on 6 Nov 2018

HAL is a multi-disciplinary open access archive for the deposit and dissemination of scientific research documents, whether they are published or not. The documents may come from teaching and research institutions in France or abroad, or from public or private research centers.

L'archive ouverte pluridisciplinaire **HAL**, est destinée au dépôt et à la diffusion de documents scientifiques de niveau recherche, publiés ou non, émanant des établissements d'enseignement et de recherche français ou étrangers, des laboratoires publics ou privés.

Linear collisionless dynamics of the GAM with kinetic electrons: comparison simulations/theory

V. Grandgirard[a], X. Garbet[a], Ch. Ehrlacher[a], Y. Asahi[b], E. Cashera[a], G. Dif-Pradalier[a], P. Donnel[a], Ph. Ghendrih[a], G. Latu[a], Ch. Passeron[a], Y. Sarazin[a], D. Zarzoso[c]

[a] *CEA, IRFM, 13108 Saint-Paul-lez-Durance Cedex, France*
[b] *National Institutes for Quantum and Radiological Science and Technology, 039-3212, Rokkasho, Aomori, Japan*
[c] *Aix-Marseille Université, CNRS, PIIM, UMR 7345 Marseille, France*

Abstract

This paper presents first comparisons of numerical gyrokinetic simulations with analytical theory to take into account the role of kinetic electrons in the damping rate of Geodesic Accoustic Modes (GAMs).

Keywords: plasma turbulence, gyrokinetic simulations, kinetic electrons, Geodesic Accoustic Mode (GAM)

1. Introduction

Zonal Flows (ZFs) and their oscillatory component, the so-called Geodesic Acoustic Mode (GAMs), play an important role in the saturation of turbulence in tokamaks. Zonal flows are an essential element to both predict and limit turbulent transport level. In 1998, Rosenbluth and Hinton [22] showed that Zonal Flows are not damped in the absence of collisions and gave an analytical estimation of the residual value for the particular case of single ion species with adiabatic electrons. GAMs have a finite frequency of the order of ion accoustic frequency. Contrary to ZFs, they can be damped by ion Landau damping, i.e via collisionless wave-particle resonance. The kinetic theory of GAMs in toroidal plasmas is well documented (see for instance [29, 25, 21] and a brief review in [20]). Analytical results have been widely compared with simulation results to validate the correct treatment of GAM and ZF time evolution in adiabatic electron versions of gyrokinetic codes (see for instance the benchmark done in [1] for ORB5 [16, 3, 2], GENE [8, 9] and GYSELA [11, 10] European codes). Until very recently there was no available theory to compute the contribution of kinetic electrons to GAM frequency and damping rate, except one model proposed for passing electrons [26]. It was numerically found that considering kinetic electrons do not really change the residual flow and collisionless frequency of GAM [5] but the damping rate is significantly enhanced by trapped kinetic electrons in regions of the tokamak where the safety factor is high ([28] with GTC [17, 13] code). Similar results have been also recovered in [14] with GT5D [15] code and in [1] with ORB5 and GENE codes. An effort to provide scaling formulae for GAM frequency and damping rate has been done [19] with ORB5 simulations.

Email address: virginie.grandgirard@cea.fr (V. Grandgirard)

An analytical estimate of the kinetic electrons contribution to GAM damping has been very recently proposed by C. Ehrlacher and al. [7]. In this analytical study, based on a variational formulation (close to the one previously used to study EGAMs [27]), it appears that barely trapped/passing electrons enhance GAM damping, while affecting weakly the real part of the GAM pulsation. In this paper we compare these analytical results to the numerical ones obtained with the semi-Lagrangian code GYSELA.

The reminder of this paper is organized as follows. In section 2, the analytical estimate of the GAM damping due to kinetic electrons used in this paper for comparison with numerical results is summarized. The global full-f gyrokinetic equations with kinetic electrons used in GYSELA code are described in section 3. Numerical results exhibiting variations of the GAM damping rate and frequency according to the ion to electron mass ratio, the electron to ion temperature ratio, the safety factor and the aspect ratio are compared to analytical results in section 4. Finally, a conclusion is given in section 5.

2. Analytical estimate of the GAM damping due to electrons

Let us consider a simplified geometry of circular concentric magnetic surfaces, labeled by their minor radius r in the toroidal coordinates (r, θ, φ). The angles (θ, φ) are the poloidal and toroidal angles. The GAM electric potential ϕ can be expanded in Fourier series with respect to the poloidal angle and minor radius

$$\phi_\omega(r,\theta) = \sum_{m=-\infty}^{+\infty} \int_{-\infty}^{\infty} \frac{\mathrm{d}k_r}{2\pi} \tilde{\phi}_{m\omega}(k_r) e^{i(k_r r + m\theta)} \tag{1}$$

where the Fourier components $\tilde{\phi}_{m\omega}(k_r)$ are determined by initial conditions. Contrary to the GAM pulsation, which is not much changed whether electrons are considered adiabatic or kinetic, numerical simulations have shown that the GAM damping could greatly depend on the kinetic response of electrons [28] and [19]. This has been recently confirmed by an analytical derivation of the total dispersion relation with electrons in [7]. This derivation was performed via the computation of the exchange of energy between the mode and electrons. The dispersion relation leads to $\bar{L} = \bar{L}_i + \bar{L}_e = 0$, where the ion contribution $\bar{L}_i$ is equivalent to that found in Sugama-Watanabe [25], namely:

$$\begin{aligned} \bar{L}_i &= k_r^2 \rho_i^2 \left|\phi_0\right|^2 \Bigg\{ \Lambda_1 - \Lambda_2 k_r^2 \rho_i^2 \\ &+ i\frac{1}{2}\sqrt{\frac{\pi}{2}} q^5 \Omega^3 e^{-\frac{q^2\Omega^2}{2}} \left[1 + 2\frac{1+2\tau_e}{q^2\Omega^2}\right] + i\frac{1}{1024}\sqrt{\frac{\pi}{2}} k_r^2 \rho_i^2 q^9 \Omega^5 e^{-\frac{q^2\Omega^2}{8}} \left[1 + 16\frac{1+\tau_e}{q^2\Omega^2}\right] \Bigg\} \end{aligned} \tag{2}$$

with q the safety factor, $\tau_e = T_e/T_i$ the electron to ion temperature ratio and where Ω is the frequency normalized to the sound frequency, namely $\Omega = \omega R/v_{Ti}$ with v_{Ti} the thermal velocity $v_{Ti} = \sqrt{T_i/m_i}$. The functions Λ_1 and Λ_2 are respectively defined as

$$\Lambda_1 = 1 - \left(\frac{7}{2} + 2\tau_e\right)\frac{1}{\Omega^2} - \left(\frac{23}{2} + 8\tau_e + 2\tau_e^2\right)\frac{1}{q^2\Omega^4} \tag{3}$$

and

$$\Lambda_2 = \frac{3}{4} - \left(\frac{13}{2} + 6\tau_e + 2\tau_e^2\right)\frac{1}{\Omega^2} + \left(\frac{747}{8} + \frac{481}{8}\tau_e + \frac{35}{2}\tau_e^2 + 2\tau_e^3\right)\frac{1}{\Omega^4} \tag{4}$$

The contribution of kinetic electrons $\bar{L}_e$ in the dispersion relation (derived in [7]) appears to be purely imaginary, so that it only affects the damping rate of GAMs, and not their real frequency, consistently with numerical findings. It is expressed as

$$\bar{L}_e = ik_r^2\rho_i^2\left|\phi_0\right|^2\left\{G(\epsilon)\eta_1^2\left(q,\tau_e\right)\mathcal{D}(\sigma^*)\left(\frac{m_e}{m_i}\right)^{1/2}\frac{q}{\tau_e^{3/2}}\Omega\right\} \tag{5}$$

with m_e/m_i the electron to ion mass ratio.

Further notice that $\bar{L}_e$ is the same positive sign as the imaginary part of $\bar{L}_i$. Consequently, one can already predict that kinetic electron effects will amplify the damping of GAMs due to ions. In the limit of large aspect ratio G is given by

$$G(\epsilon) = \sqrt{\frac{\pi}{2}}\int_0^{+\infty} d\kappa\kappa\frac{\tau^2(\kappa)}{\Lambda(\kappa,\epsilon)}\sin^2\left(\theta_0(\kappa)\right) \tag{6}$$

where θ_0 is the poloidal angle at the turning point ($\theta_0 = \pi$ for passing particles) and

$$\kappa = \sqrt{\frac{2\epsilon\lambda}{1-\lambda(1-\epsilon)}} \quad ; \quad \Lambda(\kappa,\epsilon) = \frac{2\epsilon + (1-\epsilon)\kappa^2}{1+\epsilon} \quad ; \quad \tau(\kappa) = \frac{1}{\pi}\left\{\begin{array}{cc} K(\kappa^2) & 0 \le \kappa \le 1 \\ \frac{2}{\kappa}K\left(\frac{1}{\kappa^2}\right) & 1 \le \kappa \le +\infty \end{array}\right. \tag{7}$$

with ϵ the inverse of the aspect ratio and K the complete elliptical function of the first kind. The function $\eta_1\left(q,\tau_e\right)$ is given by

$$\eta_1\left(q,\tau_e\right) = -\left[1 + \frac{2+\tau_e}{q^2\Omega^2} + o\left(\frac{1}{q^4\Omega^4}\right)\right]\frac{\tau_e}{\Omega} + o(k_r\rho_i) \tag{8}$$

The dimensionless parameter σ^*, defined as

$$\sigma^* = \left(\frac{m_e}{m_i\tau_e}\right)^{1/2}\frac{q}{\epsilon^{1/2}}\Omega \tag{9}$$

characterizes the resonance of a GAM with barely trapped/passing electrons. The form factor $\mathcal{D}(\sigma^*)$ measures the weight of the region in the phase space where $\sigma^*\tau(\kappa)\Lambda^{1/2}(\kappa)/v > 1$, i.e. the number of near resonant particles. Normalisations are such that $\mathcal{D}(\sigma^*) = 1$ when bounce points of trapped electrons play a prominent role in the electron contribution. In the most general case, one expects that $\mathcal{D}(\sigma^*) \le 1$.

Figure 1 shows a good agreement of GYSELA simulations with these theoretical resonant curves. As described in [7], considering that $\Lambda(\kappa)$ is smooth near $\kappa = 1$ with $\Lambda(1) = 1$; using the fact that a numerical estimate of $G(\epsilon)$ gives $G(\epsilon) \simeq 0.63 + 0.60\epsilon$ in the range $\epsilon < 0.3$ and using a perturbative calculation, a rough estimate of the normalized damping rate due to electrons can be expressed as

$$\frac{R_0\gamma^{\text{elec}}}{v_{Ti}} \simeq (0.315 + 0.30\epsilon)\left(1 + \frac{2+\tau_e}{q^2\Omega_0^2}\right)^2 q\tau_e^{1/2}\mathcal{D}(\sigma^*)\left(\frac{m_e}{m_i}\right)^{1/2} \tag{10}$$

with v_{Ti} the ion thermal velocity. The GAM frequency Ω_0 (solution of $Re(\bar{L}) = 0$) is a function of q and τ_e. For comparison with numerical results which follows this value is taken as the numerical

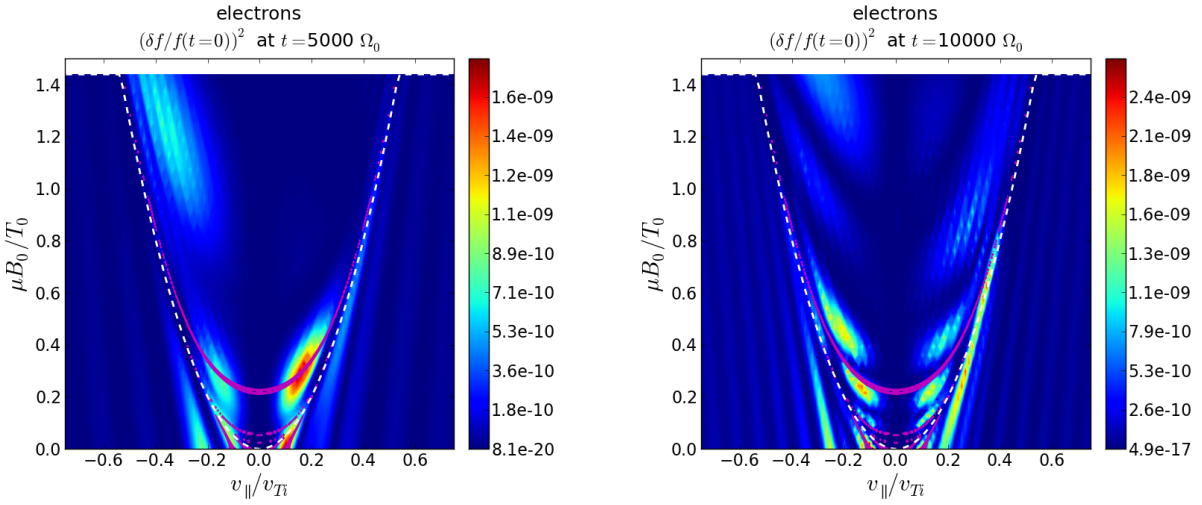

Figure 1: Contour plot of the resonant curves $\sigma^* \tau(\kappa)\Lambda^{1/2}(\kappa) = n_2 v$ (magenta lines) with the simulation results of $\delta f_e/f_{e0}$ (f_e being the electron distribution function) in $(v_\parallel, \mu)$ space for two simulation times : (left) $t = 5000\Omega_{c_0}$ and (right) $t = 10000\Omega_{c_0}$. White dotted line (corresponding to $\frac{1}{2}v_\parallel^2 = \mu(B_{\max} - B(r,\theta))$ delimit the trapping domain. Simulation parameters are equivalent to Table 2 except for the mesh discretization which is finer in velocity space, namely $(N_{v_\parallel}, N_\mu) = (1024, 64)$.

frequency given by the gyrokinetic simulations. As proposed in the following (see sections 4.3, 4.4 and 4.5), a way to validate this analytical expression Eq.(10) is to perform first a scan on one parameter among m_i/m_e, τ_e or q to determine the unknown weight function $\mathcal{D}(\sigma^*) \leq 1$ and then to check the dependency on other parameters .

3. Gyrokinetic models

3.1. GYSELA gyrokinetic global full-f model

The gyrokinetic global full-f model implemented in GYSELA code is briefly described in this section. It has the particularity to be based on an semi-Lagrangian scheme [24]. A complete description of the code both in terms of numerics and high performance computing can be found in the paper [10] as reference. Let us consider the gyro-center coordinate system $(\mathbf{x}_G, v_\parallel, \mu_s; t)$ where $\mathbf{x}_G$ corresponds to the 3D toroidal space coordinates, *i.e* $\mathbf{x}_G = (r, \theta, \varphi)$ with r the radial position, θ the poloidal angle and φ toroidal angle. $(v_\parallel, \mu_s)$ corresponds to the 2D velocity space where $v_\parallel$ is the velocity parallel to the magnetic field $\mathbf{B}$ and $\mu_s = m_s v_\perp^2/(2B)$ is the magnetic moment where $v_\perp$ is the velocity in the perpendicular direction to $\mathbf{B}$. m_s is the mass of species s. The magnetic topology is fixed and consists of concentric toroidal magnetic surfaces with circular poloidal cross-sections. Therefore, the magnetic field $\mathbf{B}$ is defined as $\mathbf{B} = (B_0 R_0/R)\,[\zeta(r)\mathbf{e}_\theta + \mathbf{e}_\varphi]$ with $R(r,\theta) = R_0 + r\cos\theta$ the major radius and $\zeta(r) = r/(qR_0)$ with $q(r)$ the safety factor. B_0 and R_0 respectively correspond to the magnetic field and the major radius of the torus, both at the magnetic axis. The vectors $\mathbf{e}_\theta = r\boldsymbol{\nabla}\theta$ and $\mathbf{e}_\varphi = R\boldsymbol{\nabla}\varphi$ are the unit vectors in the poloidal and toroidal periodic directions, respectively. Regarding the current, it is decoupled from the field and the magnetic field is assumed

to satisfy the Ampere's equation, but not the force balance equation. Then Ampere's law leads to a current of the form $\mu_0\mathbf{J} = \mu_0 J_T R\boldsymbol{\nabla}\varphi$ with $\mu_0 J_T = \frac{B_0 R_0}{R}\frac{\zeta}{r}\left(1 + \frac{r}{\zeta}\frac{\mathrm{d}\zeta}{\mathrm{dr}} - \frac{r}{R}\cos\theta\right)$.

Let $F_s(\mathbf{x}_G, v_\parallel, \mu_s; t)$ be the particle distribution function of species s at time t and $\bar{F}_s$ the one associated to the guiding-centers. The global gyrokinetic code GYSELA models for each species s, the time evolution of the guiding-center distribution function $\bar{F}_s$, with no separation between equilibrium and perturbation. The non-linear time evolution of $\bar{F}_s$ is governed by the 5D collisional gyrokinetic equation described by Brizard and Hahm [4]

$$B^*_{\parallel s}\frac{\partial \bar{F}_s}{\partial t} + \boldsymbol{\nabla}\cdot\left(B^*_{\parallel s}\frac{\mathrm{d}\mathbf{x}_G}{\mathrm{d}t}\bar{F}_s\right) + \frac{\partial}{\partial v_\parallel}\left(B^*_{\parallel s}\frac{\mathrm{d}v_\parallel}{\mathrm{d}t}\bar{F}_s\right) = B^*_{\parallel s}\left(\sum_{s'}\mathcal{C}(\bar{F}_s, \bar{F}_{s'}) + \mathcal{S}_f\right) \tag{11}$$

For more details on the multi-species collision operator $\mathcal{C}(\bar{F}_s, \bar{F}_{s'})$ including accurate treatment of ion-electron collisions see [6]. Source term $\mathcal{S}_f$ description can be found in [23, 10]. In the present paper we only consider non collisional simulations without sources. The evolution of the gyro-center coordinates of species s is described by:

$$\frac{\mathrm{d}x^i_G}{\mathrm{d}t} \equiv v_\parallel \mathbf{b}^*_s\cdot\boldsymbol{\nabla}x^i_G + \mathbf{v}_{E\times B_s}\cdot\boldsymbol{\nabla}x^i_G + \mathbf{v}_{D_s}\cdot\boldsymbol{\nabla}x^i_G \tag{12}$$

$$\frac{\mathrm{d}v_\parallel}{\mathrm{d}t} \equiv \frac{1}{m_s}\left(-\mu_s\mathbf{b}^*_s\cdot\boldsymbol{\nabla}B - q_s\mathbf{b}^*_s\cdot\boldsymbol{\nabla}\bar{\phi} + \frac{m_s v_\parallel}{B}\mathbf{v}_{E\times B_s}\cdot\boldsymbol{\nabla}B\right) \tag{13}$$

where $\mathbf{b}^*_s$ is defined as

$$\mathbf{b}^*_s = \frac{\mathbf{B}}{B^*_{\parallel s}} + \frac{m_s v_\parallel}{q_s B^*_{\parallel s} B}\boldsymbol{\nabla}\times\mathbf{B} \tag{14}$$

with $B^*_{\parallel s} = \mathbf{B}^*_s\cdot\mathbf{b}$ and $\mathbf{B}^*_s$ given by $\mathbf{B}^*_s \equiv \mathbf{B} + \frac{m_s}{q_s}v_\parallel\boldsymbol{\nabla}\times\mathbf{b}$, $\mathbf{b} = \mathbf{B}/\|B\|$ being the unit vector along the magnetic field line at the guiding-center position. The i-th contravariant components of the '$\mathbf{E}\times\mathbf{B}$' drift and of the 'grad–B' and 'curvature' drifts read

$$\mathbf{v}_{E\times B_s}\cdot\boldsymbol{\nabla}x^i_G = \frac{1}{B^*_{\parallel s}}\left[\bar{\phi}, x^i_G\right] \quad ; \quad \mathbf{v}_{D_s}\cdot\boldsymbol{\nabla}x^i_G = \left(\frac{m_s v^2_\parallel + \mu_s B}{q_s B^*_{\parallel s} B}\right)\left[B, x^i_G\right] \tag{15}$$

with the Poisson Bracket $[F, G] = \mathbf{b}\cdot(\boldsymbol{\nabla}F\times\boldsymbol{\nabla}G)$. $\bar{\phi} = \mathcal{J}_{\mu_s}.\phi$ is the gyro-average of the fluctuating electrostatic potential ϕ, i.e $\mathcal{J}_{\mu_s}.\phi = \oint_0^{2\pi}\phi\frac{\mathrm{d}\varphi_{c_s}}{2\pi}$, where φ_{c_s} stands for the cyclotron phase. The gyrokinetic equation Eq.(11) is self-consistently coupled to a quasi-neutrality equation whose expression depends on the numerical treatment of electrons. Until recently, electrons were assumed adiabatic in GYSELA code. There exist now two new models for electron treatment: (i) the first one where all electrons are treated kinetically (called "full kinetic electron" (FKE) model) and (ii) the second one where only trapped electrons are considered kinetic while passing electrons are still assumed adiabatic (called "trapped kinetic electron" (TKE)). For both models, the full-f gyrokinetic equation Eq.(11) is solved for all electrons with no distinction between trapped and passing particles. In this paper we use the FKE model, therefore the quasi-neutrality equation reads

$$\sum_i Z_i\left(n_{Gi} + n_{\mathrm{pol},i}\right) = n_{Ge} + n_{\mathrm{pol},e} \tag{16}$$

where the gyrocentre and polarization densities are defined, respectively, by

$$n_{Gs} = \int \mathrm{d}\mathbf{v}\ \mathcal{J}_{\mu_s}.\delta\bar{F}_s \quad ; \quad n_{\mathrm{pol},s} = \boldsymbol{\nabla}_\perp\cdot\left(\frac{n_{s_0}}{B_0\Omega_s}\boldsymbol{\nabla}_\perp\phi\right) \tag{17}$$

Note that, for real-mass electrons, both the gyro-average and the polarization density can be neglected for electrons. The GYSELA code is written in SI units and uses a thermal energy scale in electron volts ($1eV = 1.6022\ 10^{-19}J$). The four fundamental dimensional normalizing quantities are: a reference ionic mass $m_0 = A_0 m_p$ (kilogram), a reference ionic charge $q_0 = Z_0 e$ (Coulomb), a reference magnetic induction B_0 (Tesla) and a reference thermal energy T_0 (eV). Here, A_0 and Z_0 are the (dimensionless) mass number and charge state of the Hydrogen and e the modulus of the electron charge. The reference ion cyclotron frequency Ω_{c_0}, the reference thermal speed v_{T_0} and the reference Larmor-radius ρ_0 are defined as $\Omega_{c_0} = Z_0\, e\, B_0/m_0$, $v_{T_0} = \sqrt{T_0/m_0}$ and $\rho_0 = v_{T_0}/\Omega_{c_0}$. Then, the normalized quantities used in the code (denoted with a hat symbol) are the following: $A_s = A_0 \hat{A}_s$ with $m_s = m_0 \hat{A}_s$, $q_s = Z_0\, e\, \hat{Z}_s$, $l = \rho_0\, \hat{l}$, $t = \hat{t}/\Omega_{c_0}$, $B = B_0 \hat{B}$, $T_s = T_0 \hat{T}_s$, $v_s = v_{T_{s0}}\, \hat{v}_s$ with $v_{T_{s0}} = v_{T_0}/\sqrt{\hat{A}_s}$, $\mu_s = (T_0/B_0)\hat{\mu}_s$ and $\phi = (T_0/Z_0 e)\hat{\phi}$ with m_s, q_s, T_s, v_s, μ_s being respectively the mass, charge, temperature, velocities and magnetic momentum associated to species s while l and t denote length and time.

4. Numerical results for Rosenbluth-Hinton simulations

The so-called "Rosenbluth-Hinton test"–which became an inescapable test for gyrokinetic codes to check the validity of ZFs and GAMs treatment– was firstly verified in 2008 for the GYSELA code. It consists in computing the linear evolution of the zonal flow component ϕ_{00} for an initial electrostatic perturbation. This initial state leads to the development of GAMs which correspond to the $(m, n) = (0, 0)$ mode coupled to side-bands $(m, n) = (\pm 1, 0)$ as a result of toroidal coupling. These GAMS are Landau-damped because of the finite poloidal wave-number of the side-band while the zonal flows relax towards a residual value which has been analytically predicted in the case of large aspect ratio and small ρ_* in [12].

4.1. Numerical parameters

Numerical parameters for all the following simulations are the same as those used in [1] for previous cross-code benchmark performed between GYSELA, ORB5 and GENE codes on the linear collisionless dynamics of the GAM. Namely for all GYSELA simulations, the value of $\rho_* = \rho_s/a$ is chosen as $\rho_* = 1/160$ (taken at the magnetic axis). The 3D toroidal space (r, θ, φ) is defined as $0 \leq r \leq a$, $0 \leq \theta \leq 2\pi$ and $0 \leq \varphi \leq 2\pi$. The velocity phase space is given by $-\mathrm{nb}_{v\mathrm{max}} v_{T_{s0}} \leq v_\parallel \leq \mathrm{nb}_{v\mathrm{max}} v_{T_{s0}}$ with $\mathrm{nb}_{v\mathrm{max}} = 7$ and $0 \leq \mu \leq \mu_{\mathrm{max}} T_0/B_0$ with $\mu_{\mathrm{max}} = 12$. The radial density profile is defined by its gradient as $\mathrm{d}\log n_{s_0}(r)/\mathrm{d}r = -\kappa_{ns_0} \cosh^{-2}\left((r - r_{\mathrm{peak}})/\Delta r_{ns_0}\right)$ with r_{peak} the radial position of maximum gradients, namely the middle of the simulation box here (i.e $r_{\mathrm{peak}} = 0.5(r_{\mathrm{max}} - r_{\mathrm{min}})$). The same analytical expression is used for the temperature with κ_{Ts_0} and Δr_{Ts_0}. Density and temperature shapes are chosen the same for both ions and electrons and quasi-constant with $\kappa_{ns_0} = \kappa_{Ts_0} = 10^{-7}$, $\Delta r_{ns_0} = 0.2$ and $\Delta r_{Ts_0} = 0.1$. The ion charge Z_i (resp. electron charge Z_e) is equal to $Z_i = 1$ (resp. $Z_e = -1$). The remaining parameters are scanned in the simulations presented in the following. In the following, the so-called "standard case" corresponds to the following set of parameters: (i) the ion to electron mass ratio is equal to $m_i/m_e = 1600$, (ii) the electron to ion temperature ratio $\tau_e = T_e/T_i$ is fixed to 1, (iii) the safety factor profile is flat with $q(r) = 3.5$ and (iv) the inverse of aspect ratio $\epsilon = a/R_0$ is chosen as $\epsilon = 0.1$. In practice, in gyrokinetic codes, the Rosenbluth-Hinton (R-H) test corresponds to initializing the distribution function $\bar{F}_s$ as a Maxwellian distribution only perturbed by a zonal component (i.e independent of the poloidal and toroidal angle) generating a scalar potential ϕ with a sine (or

more rarely a cosine) dependence on the radius r. One of the difficulties of R-H tests for global codes (compared to local ones) is to preserve the radial initial structure of the zonal component in time. As described in [1], for GYSELA code the cosine structure $\phi(r, t = 0) = 1 - \cos(k_r r)$ is preferred because more stable in time (see time evolution in Figure 2) than the standard one $\phi(r, t = 0) = \sin(k_r r)$. So the distribution function is initialized as $\bar{F}_s = \bar{F}_{s,\mathrm{eq}}(1 + \epsilon_0(1 - \cos(k_r r))$ with $k_r \rho_s = 2\pi\rho_* \simeq 0.039$ and a perturbation amplitude ϵ_0 equal to 10^{-7} in this paper. For

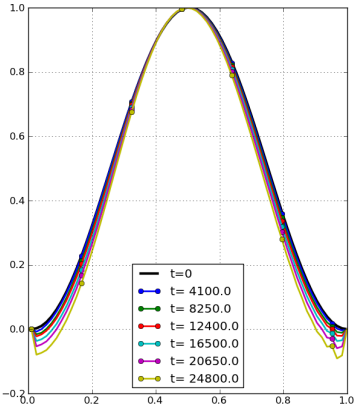

Figure 2: Radial structure of the electrostatic potential ϕ at different simulation times for a GYSELA simulation with parameters given in Table 2. $k_r \rho_i \simeq 0.039$ is almost preserved between initial time (black line) and final time $t = 24800\Omega_{c_0}$.

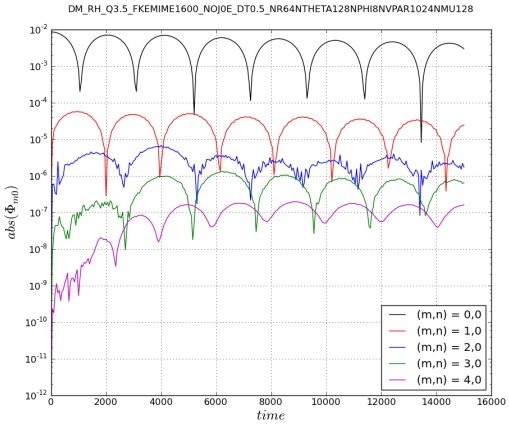

Figure 3: Time evolution of the five Fourier modes of the electrostatic potential $\tilde{\phi}_{m0}(r = 0.5a, t)$ with $m = \{0, 1, 2, 3, 4\}$ for a simulation which parameters are described in Table 2.

the following the damping rate will be approximated by the slope of the best fitting line of the maximum values of $\log(\phi(r_p, t) - \langle\phi_{00}\rangle_r(t))$ with $\langle\cdot\rangle_r$ the radial average (see Figure 4 (a) for an example with the previous reference parameters). The frequency amplitude will be approximated by the maximum value of the Fourier transform in time of $\phi(r_p, t)$ (see Figure 4 (b)). Finally, the time evolution of the five Fourier modes of the electrostatic potential $\phi_{m0}(r = 0.5a, t)$ for $m = \{0, 1, 2, 3, 4\}$ is plotted in Figure 3. This confirms that conserving only the first harmonics $m = 0, \pm 1$ of the potential in the analytical derivation in [7] to obtain the simplified analytical expression (5) is licit. Indeed, as already found analytically (cf. Appendix C of Nguyen's thesis [18] or [25]) we recover that $\tilde{\phi}_{m\omega}(k_r)$ scales approximately as $(-ik_r\rho_i)^m \tilde{\phi}_{0\omega}$.

4.2. Convergence tests

Convergence tests in space and time have already been performed with the GYSELA code in the case of adiabatic electrons in [11]. Let N_x be the number of points in x direction, then it appeared that the best compromise is a 5D mesh $(N_r, N_\theta, N_\varphi, N_{v_\parallel}, N_\mu) = (64, 64, 8, 128, 8)$ with a time step $\Omega_{c_0}\Delta t = 25$. Knowing that fully kinetic electrons simulations are more demanding in terms of mesh and time discretization, the same kind of convergence study has been completed for a relatively large mass ratio $m_i/m_e = 1600$. At such mass ratio, previous simulations have shown that a time discretization equal to $\Delta t = 0.5\Omega_{c_0}^{-1}$ is reasonable. So Δt is fixed at this value for the whole convergence study. As for adiabatic electrons, the number of toroidal points N_φ is fixed to $N_\varphi = 8$ due to the toroidal axisymmetry of the test. Finally, the convergence study consists in

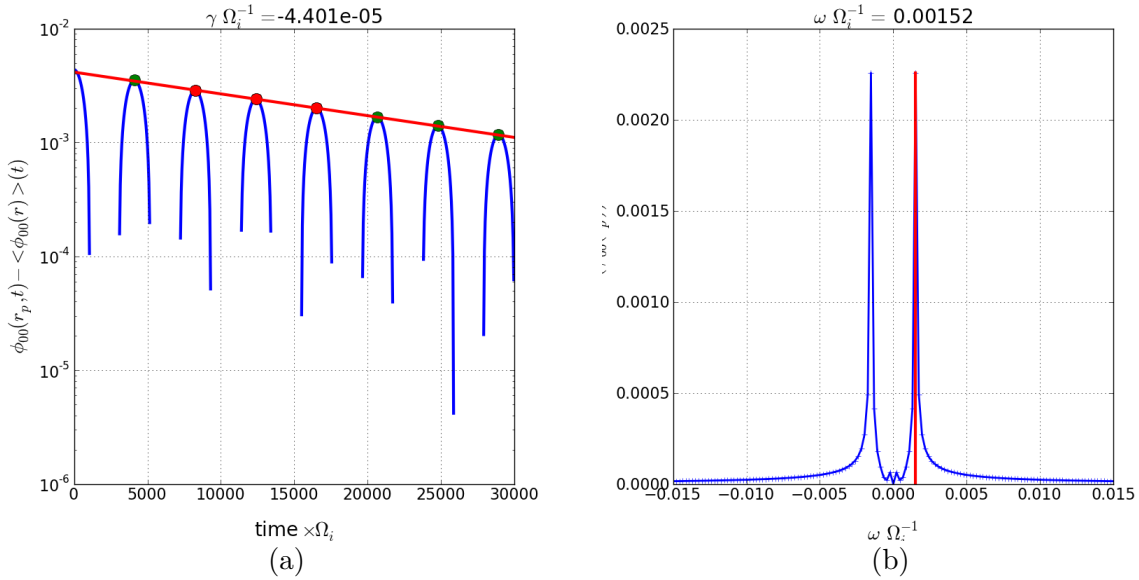

Figure 4: Simulation results for numerical parameters given in Table 2: (a) Time evolution of $\log(\phi(r_p,t) - \langle\phi_{00}\rangle_r(t))$ ($r_p = 0.5a$) with an approximate value of the damping rate $\gamma\Omega_{c_0}^{-1} \simeq 4.4\ 1e^{-5}$ given by the slope of the red line ; (b) Fourier transform in time of $\phi(r_p,t)$ which gives an approximation of the GAM frequency equal to $\omega\Omega_{c_0}^{-1} \simeq 0.0015$.

13 simulations where the 4 mesh discretization parameters $(N_r, N_\theta, N_{v_\parallel}, N_\mu)$ vary. The results for damping rate $\gamma_{\rm GAM}$, frequency $\omega_{\rm GAM}$ and time average of $k_r\rho_i$ are summarized in Table 1. Each simulation corresponds to 60000 iterations, so these three quantities are computed from initial time $t = 0$ to final time $t = 30000\,\Omega_{c_0}^{-1}$. All simulations have been performed on Skylake partition of Marconi supercomputer (CINECA/Bologna) with 24 threads and N_μ MPI process (see [11] for detailed OpenMP/MPI parallelization of the code). The poloidal discretization is almost always the same for all simulations: $(N_r, N_\theta) = (64, 128)$ except one with $(N_r, N_\theta) = (128, 256)$. Indeed, by comparing simulations 7 and 13 in Table 1, we see that increasing the number of points by a factor 2 in both directions r and θ does not change significantly the $\gamma_{\rm GAM}$ value. So more attention is paid to the velocity phase space discretization where $N_{v_\parallel}$ varies in power of 2 from 128 to 1024 and N_μ from 32 to 128. With a mean value equal to $\langle\omega_{\rm GAM}\rangle \simeq 0.001524$ and a standard deviation $\sigma(\omega_{\rm GAM}) = 4.2\,e^{-6}$, the frequency is not affected by the mesh discretization. In the same way, the time average of $k_r\rho_i$ is almost unchanged (mean value: 0.03908, standard deviation: $8.3\,e^{-5}$). Conversely as expected, the damping rate is more affected. It seems more sensitive to the number of points in $v_\parallel$ direction. Indeed, independently of the number of points in μ direction, $\gamma_{\rm GAM}$ is 40% larger with $N_{v_\parallel} = 128$ than with $N_{v_\parallel} \geq 512$. From this analysis, we consider that using a 5D mesh of $(N_r, N_\theta, N_\varphi, N_{v_\parallel}, N_\mu) = (64, 128, 8, 512, 64)$ is a good compromise between accuracy and CPU cost. Thus, all following simulations are performed with such a mesh of 2.14 billions of points, requiring $\sim 150k$ hours/monoprocessor for $60k$ iterations. The main parameters of what will be called in the following *standard R-H case* are summarized in Table 2.

4.3. Dependency on the ion to electron mass ratio m_i/m_e

Previous simulations performed both with ORB5 and GENE codes indicate that the damping rate due to trapped electrons scales as $(m_e/m_i)^{1/2}$ [1]. This suggests that $\mathcal{D}(\sigma^*)$ is constant and close to $\mathcal{D}(\sigma^*) \simeq 1.0$. Such a scan in m_i/m_e (varying from $m_i/m_e = 100$ to the more realistic

simu.	N_r	N_θ	$N_{v_\parallel}$	N_μ	$\gamma_{\rm GAM}(\sqrt{2}v_{Ti}/R)$	$\omega_{\rm GAM}(\sqrt{2}v_{Ti}/R)$	$\langle k_r\rho_i\rangle_t$	CPU time (h./monoproc.)
1	64	128	128	32	-0.00002541001	0.00153248422	0.03906082336	16184.26
2	64	128	255	32	-0.00003999614	0.00152071958	0.03906082032	38375.69
3	64	128	512	32	-0.00004367136	0.00152256142	0.03906082012	76835.65
4	64	128	1024	32	-0.00004360795	0.00152256142	0.03906082011	156134.16
5	64	128	128	64	-0.00002620166	0.00153093312	0.03906082331	32985.67
6	64	128	255	64	-0.00003985935	0.00152071958	0.03906082026	78809.84
7	64	128	512	64	-0.00004371152	0.00152256142	0.03906082006	156300.98
8	64	128	1024	64	-0.00004401435	0.00152256142	0.03906082005	317991.70
9	64	128	128	128	-0.00002619368	0.00153093312	0.03906082328	70301.22
10	64	128	255	128	-0.00003986099	0.00152071958	0.03906082023	158906.56
11	64	128	512	128	-0.00004381998	0.00152256142	0.03906082003	315340.87
12	64	128	1024	128	-0.00004400764	0.00152256142	0.03906082002	639803.72
13	128	256	512	64	-0.00004309582	0.00152412071	0.03936013940	406066.57

Table 1: Values of numerical damping $\gamma_{\rm GAM}$, frequency $\omega_{\rm GAM}$ and time average $\langle k_r\rho_i\rangle_t$ for 13 R-H simulations with GYSELA code (using reference parameter defined in section 4.1, i.e $\rho_* = 1/160$, $\epsilon = 0.1$, $q = 3.5$, $m_i/m_e = 1600$ and $\tau_e = 1$) varying according to the 4 mesh discretization $(N_r, N_\theta, N_{v_\parallel}, N_\mu)$ while N_φ is fixed to $N_\varphi = 8$. The time discretization is also a fixed parameter such as $\Delta t = 0.5\Omega_{c_0}^{-1}$. The last column corresponds to CPU time in hours/monoprocessor per simulation on Marconi Skylake partition.

ρ_*	$\epsilon_0 = a/R_0$	Z_i	Z_e	A_i	A_i/A_e	$q(r)$	$\tau_e = T_e/T_i$	κ_{ns_0}	Δr_{ns_0}	κ_{Ts_0}	Δr_{Ts_0}
1/160	0.1	1	-1	1.	1600.	3.5	1.	1.e^{-7}	0.2	1.e^{-7}	0.1
L_r	L_θ	L_φ	nb$_{v\rm max}$	$\mu_{\rm max}$	N_r	N_θ	N_φ	$N_{v_\parallel}$	N_μ	$\Omega_{c_0}\Delta t$	
$1/\rho_*$	2π	2π	7.	12.	64	128	8	512	64	0.5	

Table 2: Standard parameters for Rosenbluth-Hinton test with fully kinetic electrons in GYSELA code. The 3D (r, θ, φ) phase space is defined as $0 \le r \le L_r\rho_0^{-1}$, $0 \le \theta \le L_\theta$ and $0 \le \varphi \le L_\varphi$. The velocity phase space is defined by $-{\rm nb}_{v\rm max}v_{T_{s0}} \le v_\parallel \le {\rm nb}_{v\rm max}v_{T_{s0}}$ and $0 \le \mu \le \mu_{\rm max}T_0/B_0$. The safety factor radial profile $q(r)$ is constant. The radial density and temperature shapes are the same for both ions and electrons and defined by their gradients as $\mathrm{d}\log y_{s_0}(r)/\mathrm{d}r = -\kappa_{ys_0}\cosh^{-2}\left((r - r_{\rm peak})/\Delta r_{ys_0}\right)$ with $y = \{n, T\}$ and $r_{\rm peak} = 0.5(r_{\rm max} - r_{\rm min})$.

value 3200) has been performed with GYSELA code and compared to the analytical result of the damping rate due to kinetic electrons given by ($\gamma^{\rm elec} = -\frac{Im(\tilde{L}_e)}{Re(\tilde{L})_{\Omega=\Omega_0}}$) as derived in Eq.(10) assuming $\mathcal{D}(\sigma^*) = 1$

$$\gamma^{\rm elec}\,(R_0\,2^{-1/2}v_{Ti}^{-1}) \simeq \sqrt{2}(0.315+0.3\epsilon)\left(1+(2+\tau_e)/(q^2\Omega_0^2)\right)^2 q\tau_e^{1/2}(m_e/m_i)^{1/2} \qquad (18)$$

For these simulations all the parameters are the same as those given in Table 2 except that the discretization time step is adapted according to the mass ratio: $\Omega_{c_0}\Delta t = 2.0$ for $m_i/m_e = 100$, $\Omega_{c_0}\Delta t = 1.0$ for $m_i/m_e = \{200, 400\}$, $\Omega_{c_0}\Delta t = 0.5$ for $m_i/m_e \in [800, 1600]$ and $\Omega_{c_0}\Delta t = 0.25$ for $m_i/m_e = \{2000, 3200\}$. Numerical results presented in Figure 5 show a good agreement between

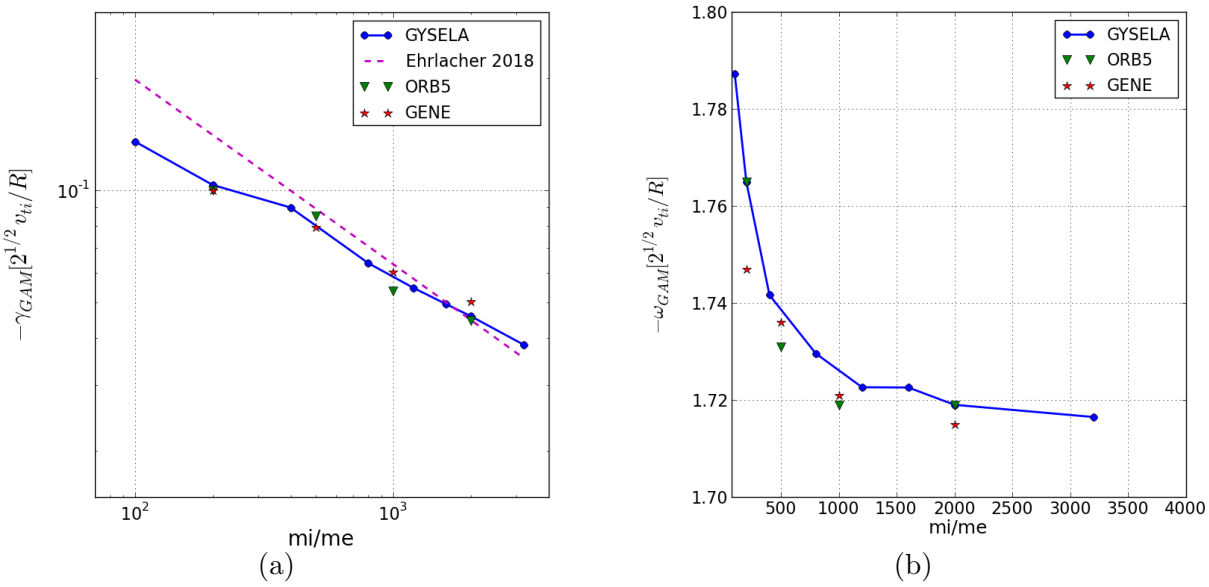

Figure 5: Damping rate (a) and frequency amplitude (b) of the radial electric field versus mi/me measured with GYSELA code (blue line) and compared to ORB5 (green triangles) and GENE (red stars) codes published in [1]. The dotted magenta line in (a) corresponds to the analytical expression of γ given by Eq.(18).

the three codes both for damping rate and frequency. On the same Figure 5 (a), we can also see a fairly good agreement amongst numerical damping rates and analytical prediction for $m_i/m_e \geq 400$. The deviation observed for smaller (less realistic) mass ratio is due to the limit of validity of the theory in this region. Indeed, at small ion to electron mass ratio it seems that most resonant particles are passing particles (see Figure 6 for $m_i/m_e = 100$). At time $t = 5000\Omega_{c_0}$ (Fig 6 (left)), most resonant particles are outside the trapping domain (region inside the white dotted line corresponding to $\frac{1}{2}v_\parallel^2 = \mu(B_{\max} - B(r,\theta))$ on the figure). This is even more evident at later time $t = 15000\Omega_{c_0}$ (see Figure 6 (right)). These results can be compared with what was previoulsy obtained for $m_i/m_e = 1600$ on Figure 1. In this situation where passing particles play the main role, the analytical expression proposed in [7] –which considers that bounce integrals are dominated by locations where particles slow down or bounce back (turning points)– is no more valid. With such parameters, the required condition $\sigma^* < 1$ is no more satisfied (i.e $\sigma^* \simeq 3.5\sqrt{0.01}\frac{1.7}{\sqrt{0.1}} = 1.88$ for $m_i/m_e = 100$) and $\mathcal{D}(\sigma^*)$ is no more equal to 1. The numerical curve is below the theoretical

one. This observation is in qualitative agreement with the theory which states that $\mathcal{D}(\sigma^*) \leq 1$ in this regime. Finally, we can also notice that the present simulation with smaller mass ratio requires less discretization in velocity space. For Figure 6, $(N_{v_\parallel}, N_\mu) = (512, 64)$ are sufficient while twice more points are required in $v_\parallel$ direction for previous Figure 1.

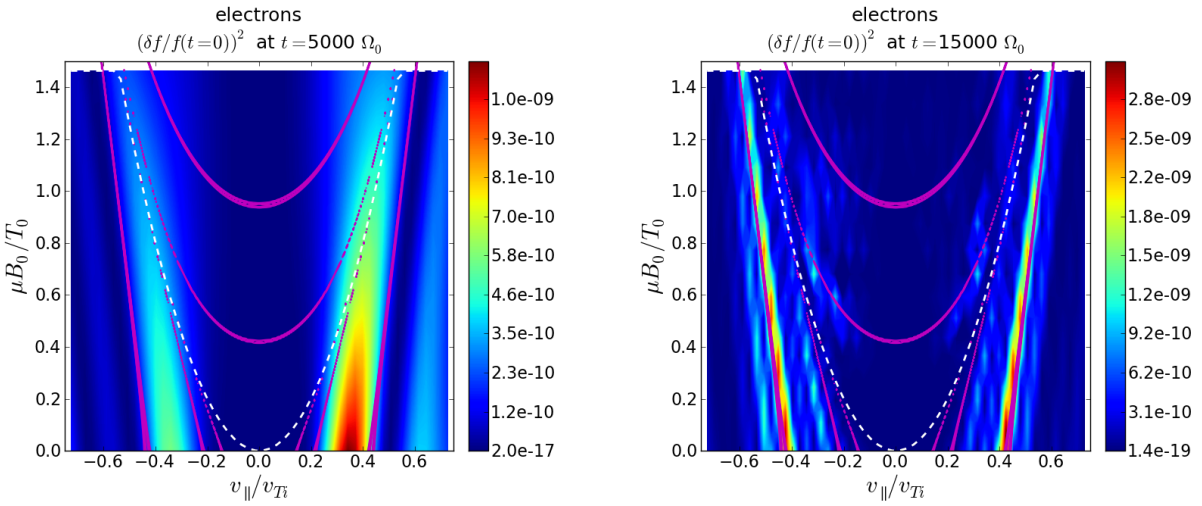

Figure 6: Contour plot of the resonant curves $\sigma^*\tau(\kappa)\Lambda^{1/2}(\kappa) = n_2 v$ (magenta lines) compared to simulation results of $\delta f_e/f_{e0}$ (f_e being the electron distribution function) in $(v_\parallel, \mu)$ space for two simulation times : (left) $t = 5000\Omega_{c_0}$ and (right) $t = 15000\Omega_{c_0}$. White dotted line (corresponding to $\frac{1}{2}v_\parallel^2 = \mu(B_{\max} - B(r,\theta))$ delimit the trapping domain. Simulation parameters correspond to Table 2 with $m_i/m_e = 100$.

4.4. Dependency on the electron to ion temperature ratio $\tau_e = T_e/T_i$

The results in previous section consolidate the dependency of the damping rate with respect to $(m_i/m_e)^{-1/2}$. We perform now a scan in $\tau_e = T_e/T_i$ to see if the variation in $\tau_e^{1/2}$ is recovered. For this, four simulations based on the parameters given in Table 2 are run by varying τ_e from 0.25 to 3.0 values. The ion temperature profile $T_i(r)$ is fixed for the four simulations while the electron temperature profile varies. Namely, $T_e(r)$ is chosen homothetic to $T_i(r)$ (i.e $\kappa_{Te_0} = \kappa_{Ti_0}$ and $\Delta r_{Te_0} = \Delta r_{Ti_0}$) and such that $T_e(r) = \tau_e T_i(r)$. Results in Figure 7 exhibit a good agreement between numerical damping rate and its analytical expression Eq.(18), especially for $\tau_e \in [0.5, 2]$. As already pointed out by previous simulations [5], we recover that the GAM frequency is not affected by non adiabatic electrons. Indeed, in Figure 7 (b) the GAM frequency is in excellent agreement with Sugama-Watanabe [25] prediction –where electron contribution is not taken into account– given by

$$\omega_{\mathrm{GAM}}^2 = \left(\frac{7+4\tau_e}{2}\right)\left(1 + \frac{23+16\tau_e+4\tau_e^2}{q^2\,(7+4\tau_e)^2}\right) \tag{19}$$

4.5. Dependency on the safety factor q

In this section, we perform a scan in q for fully kinetic electrons (FKE) GYSELA simulations with the same parameters as previously (see Table 2) where only the safety factor value is changed

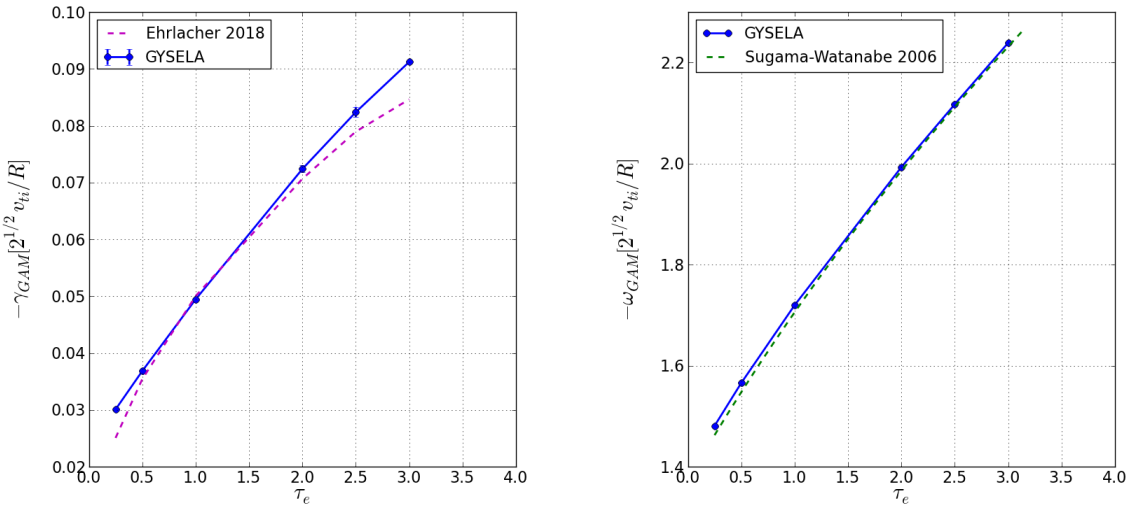

Figure 7: Damping rate (a) and frequency amplitude (b) of the radial electric field versus τ_e measured with GYSELA code (blue line). The dotted magenta line in (a) corresponds to the analytical expression of γ given by Eq.(18) while the dotted green line in (b) is the analytical prediction given by Sugama & Watanabe in [25].

$q = [1.5, 2, 3, 3.5, 4, 5]$. The results for the GAM damping rate (blue solid line) are reported and compared with analytical expressions (dotted lines) in Figure 9. There are two different regions depending on wether the safety factor is smaller or larger than $q = 3.5$. For q values larger than 3.5, the trend is close to the analytical expression but the agreement is better if $\mathcal{D}(\sigma^*)$ is taken equal to 0.94 in Equation (10) (red dotted line in Fig. 9) instead of $\mathcal{D}(\sigma^*) = 1$ (magenta dotted line in Fig. 9) as assumed until now. For q values smaller than 3.5, there is no match between theory and simulation. This is expected since at low q values, the damping due to ions is no longer negligible. Indeed, if we compare these simulations (GYSELA FKE: blue points in Fig. 8 (a)) with the six same simulations but where electrons are assumed adiabatic (GYSELA AE: red points in Fig. 8 (a)) we observe that the ratio of the GAM damping rate between FKE and AE simulations varies from a few units for $q \leq 2$ to a few tens for larger safety factors ($\gamma^{\rm FKE}_{\rm GAM}/\gamma^{\rm AE}_{\rm GAM} \simeq [2.33, 3.1, 6.89, 14.0, 31.27, 64.73]$ for $q = [1.5, 2, 3, 3.5, 4, 5]$). Pursuing this idea, if we subtract the contribution of ions –given by the adiabatic electrons simulations– to the fully kinetic electron simulations we see (black points in Figure 9) that the agreement with the analytical expression is clearly improved for $2 < q \leq 5$ with a deviation of 6%. For q smaller than 2 we meet the same limitations as the ones observed for analytical/simulation comparisons in the case of adiabatic electrons (see Fig. 3 in Biancalani's paper [1]). The differences between the GYSELA simulations with adiabatic electrons performed in paper [1] and the ones plotted in Figure 8 only deal with the adopted mesh sizes: the (r, θ, φ) mesh is coarser in present GYSELA simulations, while the mesh is finer in the velocity space. Therefore, the deviation of the numerical values to Equation (10) for $q < 2$ could be partly explained by the deviation already observed with Sugama-Watanabe damping rate estimation [25] in the case of adiabatic electrons.

Finally, let us notice that we recover once again (see Figure 8 (b)) the fact that the GAM frequency is not affected by electrons. Indeed, results between GYSELA fully kinetic electron

simulations (blue solide line) and adiabatic electron simulations (red solid line) are much the same and comparable to Sugama-Watanabe expression [25] (green dotted line).

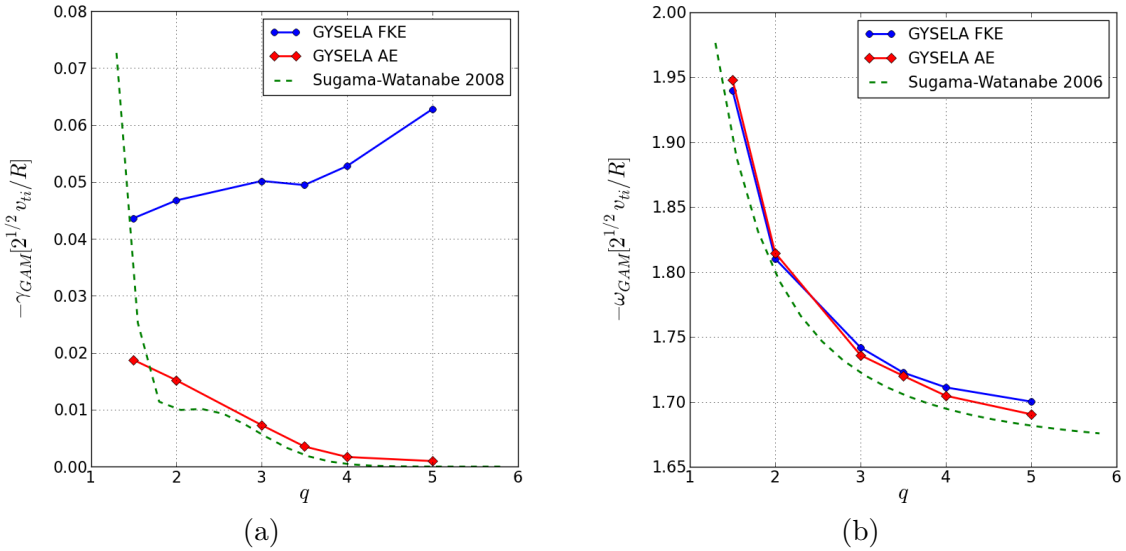

Figure 8: Damping rate (a) and frequency (b) of the radial electric field versus the safety factor q measured with GYSELA code for two types of simulations: adiabatic electrons (GYSELA AE-red line) and kinetic electrons (GYSELA FKE-blue line). The dotted green lines correspond to the explicit formulas of the damping rate and the frequency given by Sugama and Watanabe in [25] (see Eq. (19)).

4.6. Dependency on aspect ratio

Finally, a last scan in aspect ratio A is done. For this, the same parameters (Table 2) are used except the aspect ratio which varies from 4. to 10. with a step of 2. We should point out that we have faced some difficulties with the smallest aspect ratio 4 and 6. The reason is not clear but these two simulations were not possible without decreasing the time step by a factor 2., i.e $\Delta t = 0.25\Omega_{c_0}^{-1}$. The results of the GAM damping rate for these four simulations are summarized in Figure 10. We see a good agreement for $A = 6$ and $A = 8$. Apart from the fact that simulations with small aspect ratio are difficult to perform, we have to keep in mind that the analytical expression derived in [7] is only valid for small $\epsilon = 1/A$. The terms in $o(\epsilon^2)$ are neglected. This could explain the discrepancy observed in Figure 10 for $A = 4$. The deviation for $A = 10$ is however less understood. Concerning the GAM frequency we recover, as predicted by the theoretical expression (19), that it does not depend on the aspect ratio. For the four GYSELA simulations, ω_{GAM} is quasi-constant with $\omega_{\mathrm{GAM}}[2^{1/2}v_{T_{s0}}/R] = 1.7198$ and a standard deviation $\sigma = 0.00374$.

5. Conclusion

Numerical simulations based on a "Rosenbluth-Hinton" test [22] have been performed with the global gyrokinetic code GYSELA including the kinetic treatment of all electrons. Results are compared with the recent analytical theory derived in [7] showing that the contribution of electrons to GAM damping in tokamak plasmas is not negligible due to a resonance between barely

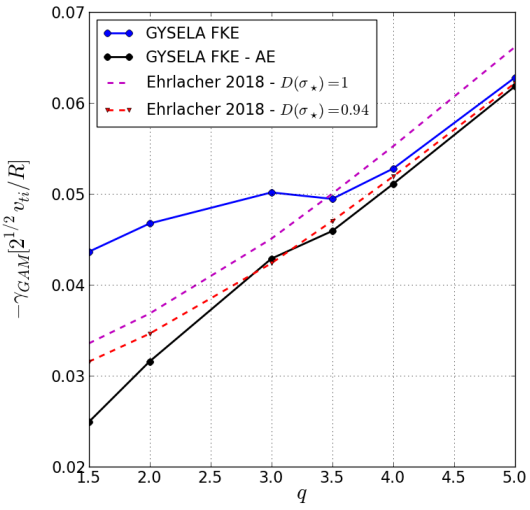

Figure 9: Damping rate of the radial electric field versus the safety factor q measured with GYSELA code (blue line). The dotted lines correspond to the analytical expression of γ given by Eq.(10): with $\mathcal{D}(\sigma^*) = 1$ (magenta line) and with $\mathcal{D}(\sigma^*) = 0.94$ (red line).

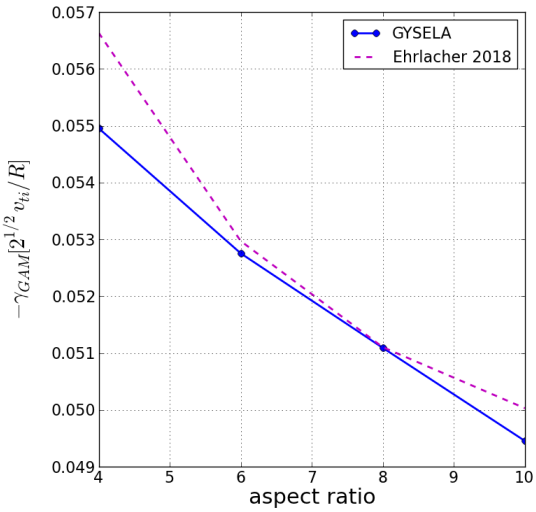

Figure 10: Damping rate of the radial electric field versus aspect ratio measured with GYSELA code (blue line). The dotted magenta line on the left graph corresponds to the analytical expression of γ given by Eq.(18).

trapped/passing electrons bounce/transit frequency and the mode pulsation. These comparisons show a fair agreement especially in the limit of the validity of the theory where trapped particles are assumed dominant. The weight function that measures the number of resonant trapped electrons participating in mode damping is found constant and equal to 1 as expected from theory. Besides, in accordance with theory and previous numerical simulations it is recovered that the GAM frequency is weakly affected by the presence of electrons.

Finally we want to point out that the tests proposed in this paper provide an interesting verification for gyrokinetic codes that deal with non adiabatic electrons.

Acknowledgments

The authors acknowledge the fruitful and lively discussions held during the Festival de Théorie in Aix-en-Provence. One of the authors (D. Z.) acknowledges support from the A*MIDEX project (no. ANR-11-IDEX-0001-02) funded by the Investissements d Avenir French Government program, managed by the French National Research Agency (ANR). This work has been carried out within the framework of the EUROfusion Consortium and has received funding from the Euratom research and training program 20142018 under Grant Agreement No. 633053, for the WP15-ER-01/IPP01 project on Verification and development of new algorithms for gyrokinetic codes. This work was supported by the Energy oriented Centre of Excellence (EoCoE), grant agreement number 676629, funded within the Horizon2020 framework of the European Union. The views and opinions expressed herein do not necessarily reflect those of the European Commission. This work was also granted access to the HPC resources of TGCC and CINES under the allocation 2018-2224 made by GENCI.

References

[1] Biancalani, A., Bottino, A., Ehrlacher, C., Grandgirard, V., Merlo, G., Novikau, I., Qiu, Z., Sonnendrücker, E., Garbet, X., Goerler, T., Leerink, S., Palermo, F., Zarzoso, D., 2017. Cross-code gyrokinetic verification and benchmark on the linear collisionless dynamics of the geodesic acoustic mode. Phys. Plasmas 24 (6), 062512.

[2] Bottino, A., Sonnendrcker, E., 2015. Monte carlo particle-in-cell methods for the simulation of the vlasovmaxwell gyrokinetic equations. Journal of Plasma Physics 81 (5), 435810501.

[3] Bottino, A., Vernay, T., Scott, B., Brunner, S., Hatzky, R., Jolliet, S., McMillan, B. F., Tran, T. M., Villard, L., 2011. Global simulations of tokamak microturbulence: finite-beta effects and collisions. Plasma Phys. Control. Fusion 53 (12), 124027.

[4] Brizard, A., Hahm, T., Apr 2007. Foundations of nonlinear gyrokinetic theory. Rev. Mod. Phys. 79 (2), 421–468.

[5] Chen, Y., Parker, S., Cohen, B., Dimits, A., Nevins, W., Shumaker, D., Decyk, V., Leboeuf, J., 2003. Simulations of turbulent transport with kinetic electrons and electromagnetic effects. Nuclear Fusion 43 (10), 1121.

[6] Donnel, P., Garbet, X., Sarazin, Y., Grandgirard, V., Asahi, Y., Bouzat, N., Caschera, E., Dif-Pradalier, G., Ehrlacher, C., Ghendrih, P., 2018. A multi-species collisional operator for full-f global gyrokinetics codes : Numerical aspects and validation with the GYSELA code. Comp. Phys. Comm.

[7] Ehrlacher, C., Garbet, X., Grandgirard, V., Sarazin, Y., Donnel, P., Caschera, E., Ghendrih, P., Zarzoso, D., 2018. Contribution of kinetic electrons to gam damping. In: Journal of Physics Conference Series. Theory of Fusion Plasmas. p. to be published.

[8] F., J., W., D., M., K., B.N., R., 2000. Electron temperature gradient driven turbulence. Phys. Plasmas 7 (5), 1904.

[9] Goerler, T., Lapillonne, X., Brunner, S., Dannert, T., Jenko, F., Merz, F., Told, D., 2011. The global version of the gyrokinetic turbulence code GENE. J. Comput. Phys. 230 (18), 7053 – 7071.

[10] Grandgirard, V., Abiteboul, J., Bigot, J., Cartier-Michaud, T., Crouseilles, N., Dif-Pradalier, G., Ehrlacher, C., Esteve, D., Garbet, X., Ghendrih, P., Latu, G., Mehrenberger, M., Norscini, C., Passeron, C., Rozar, F., Sarazin, Y., Sonnendrücker, E., Strugarek, A., Zarzoso, D., 2016. A 5D gyrokinetic full-f global semi-lagrangian code for flux-driven ion turbulence simulations. Computer Physics Communications 207, 35–68.

[11] Grandgirard, V., Brunetti, M., Bertrand, P., Besse, N., Garbet, X., Ghendrih, P., Manfredi, G., Sarazin, Y., Sauter, O., Sonnendrcker, E., Vaclavik, J., Villard, L., 2006. A drift-kinetic semi-lagrangian 4D code for ion turbulence simulation. Journal of Computational Physics 217 (2), 395 – 423.

[12] Hinton, F., Rosenbluth, M., 1999. Dynamics of axisymmetric ExB and poloidal flows in tokamaks. Plasma Phys. Control Fusion 41.

[13] Holod, I., Zhang, W. L., Xiao, Y., Lin, Z., 2009. Electromagnetic formulation of global gyrokinetic particle simulation in toroidal geometry. Physics of Plasmas 16 (12), 122307.

[14] Idomura, Y., 2016. A new hybrid kinetic electron model for full-f gyrokinetic simulations. J. Comput. Phys. 313 (C), 511–531.

[15] Idomura, Y., Ida, M., Kano, T., Aiba, N., Tokuda, S., 2008. Conservative global gyrokinetic toroidal full-f five-dimensional Vlasov simulation. Comp. Phys. Comm 179 (6), 391–403.

[16] Jolliet, S., Bottino, A., Angelino, P., Hatzky, R., Tran, T. M., Mcmillan, B., Sauter, O., Appert, K., Idomura, Y., Villard, L., 2007. A global collisionless PIC code in magnetic coordinates. Comp. Phys. Comm 177 (5), 409 – 425.

[17] Lin, Z., Hahm, T. S., Lee, W. W., Tang, W. M., White, R. B., 1998. Turbulent transport reduction by Zonal Flows: Massively parallel simulations. Science 281 (5384), 1835–1837.

[18] Nguyen, C., Oct. 2009. Magneto-hydrodynamic activity and energetic particles : application to beta alfven eigenmodes. Ph.D. thesis, Ecole polytechnique, Palaiseau.

[19] Novikau, I., Biancalani, A., Bottino, A., Conway, G., Gürcan, O., Manz, P., Morel, P., Poli, E., Di Siena, A., 2017. Linear gyrokinetic investigation of the geodesic acoustic modes in realistic tokamak configurations. Phys. Plasmas 24 (12), 122117.

[20] Qiu, Z., Chen, L., Zonca, F., 2018. Kinetic theory of geodesic acoustic modes in toroidal plasmas: a brief review. Plasma Science and Technology 20 (9), 094004.

[21] Ren, H., 2017. Finite-orbit-width effects on the geodesic acoustic mode in the toroidally rotating tokamak plasma. Physics of Plasmas 24 (5), 054504.

[22] Rosenbluth, M., Hinton, F., 1998. Poloidal flow driven by Ion-Temperature-Gradient turbulence in tokamaks. Phys. Rev. Lett. 80 (4).

[23] Sarazin, Y., Grandgirard, V., Abiteboul, J., Allfrey, S., Garbet, X., Ghendrih, P., Latu, G., Strugarek, A., Dif-Pradalier, G., Diamond, P., Ku, S., Chang, C., McMillan, B., Tran, T., Villard, L., Jolliet, S., Bottino,

A., Angelino, P., 2011. Predictions on heat transport and plasma rotation from global gyrokinetic simulations. Nuclear Fusion 51 (10), 103023.
[24] Sonnendrücker, E., Roche, J., Bertrand, P., Ghizzo, A., 1999. The semi-Lagrangian method for the numerical resolution of Vlasov equation. J. Comput. Phys. 149 (2), 201–220.
[25] Sugama, H., Watanabe, T.-H., 2008. Erratum: collisionless damping of geodesic acoustic modes [j. plasma physics (2006) 72, 825]. Journal of Plasma Physics 74 (1), 139140.
[26] Wang, L., Dong, J. Q., Shen, Y., He, H. D., 2011. Effects of electron dynamics on kinetic geodesic acoustic mode in tokamak plasmas. Plasma Physics and Controlled Fusion 53 (9), 095014.
[27] Zarzoso, D., Garbet, X., Sarazin, Y., Dumont, R., Grandgirard, V., 2012. Fully kinetic description of the linear excitation and nonlinear saturation of fast-ion-driven geodesic acoustic mode instability. Phys. Plasmas 19 (2).
[28] Zhang, H., Lin, Z., 2010. Trapped electron damping of geodesic acoustic mode. Phys. Plasmas 17, 072505.
[29] Zonca, F., Chen, L., Santoro, R., 1996. Kinetic theory of low-frequency alfvn modes in tokamaks. Plasma Physics and Controlled Fusion 38 (11), 2011.